Atmos. Chem. Phys., 15, 7765–7776, 2015
www.atmos-chem-phys.net/15/7765/2015/
doi:10.5194/acp-15-7765-2015

Atmospheric Chemistry and Physics Open Access

Phase partitioning and volatility of secondary organic aerosol components formed from α-pinene ozonolysis and OH oxidation: the importance of accretion products and other low volatility compounds

F. D. Lopez-Hilfiker[1], C. Mohr[1,7], M. Ehn[2,3], F. Rubach[3], E. Kleist[4], J. Wildt[4], Th. F. Mentel[3], A. J. Carrasquillo[5], K. E. Daumit[5], J. F. Hunter[5], J. H. Kroll[5], D. R. Worsnop[2,6], and J. A. Thornton[1,2,3]

[1]Department of Atmospheric Sciences, University of Washington, Seattle, WA, 98195, USA
[2]Department of Physics, P.O. Box 64, 00014, University of Helsinki, Helsinki, Finland
[3]Institute for Energy and Climate Research (IEK-8), Forschungszentrum Jülich, 52425 Jülich, Germany
[4]Institute of Bio-Geosciences (IBG-2), Forschungszentrum Jülich, 52425 Jülich, Germany
[5]Department of Civil and Environmental Engineering, Massachusetts Institute of Technology, Cambridge, MA 02139, USA
[6]Center for Aerosol and Cloud Chemistry, Aerodyne Research, Inc., Billerica, MA, USA
[7]Institute for Meteorology and Climate Research, Karlsruhe Institute of Technology, 76344 Eggenstein-Leopoldshafen, Germany

Correspondence to: J. A. Thornton (thornton@atmos.washington.edu)

Received: 27 January 2015 – Published in Atmos. Chem. Phys. Discuss.: 18 February 2015
Revised: 28 May 2015 – Accepted: 16 June 2015 – Published: 16 July 2015

Abstract. We measured a large suite of gas- and particle-phase multi-functional organic compounds with a Filter Inlet for Gases and AEROsols (FIGAERO) coupled to a high-resolution time-of-flight chemical ionization mass spectrometer (HR-ToF-CIMS) developed at the University of Washington. The instrument was deployed on environmental simulation chambers to study monoterpene oxidation as a secondary organic aerosol (SOA) source. We focus here on results from experiments utilizing an ionization method most selective towards acids (acetate negative ion proton transfer), but our conclusions are based on more general physical and chemical properties of the SOA. Hundreds of compounds were observed in both gas and particle phases, the latter being detected by temperature-programmed thermal desorption of collected particles. Particulate organic compounds detected by the FIGAERO–HR-ToF-CIMS are highly correlated with, and explain at least 25–50 % of, the organic aerosol mass measured by an Aerodyne aerosol mass spectrometer (AMS). Reproducible multi-modal structures in the thermograms for individual compounds of a given elemental composition reveal a significant SOA mass contribution from high molecular weight organics and/or oligomers (i.e., multi-phase accretion reaction products). Approximately 50 % of the HR-ToF-CIMS particle-phase mass is associated with compounds having effective vapor pressures 4 or more orders of magnitude lower than commonly measured monoterpene oxidation products. The relative importance of these accretion-type and other extremely low volatility products appears to vary with photochemical conditions. We present a desorption-temperature-based framework for apportionment of thermogram signals into volatility bins. The volatility-based apportionment greatly improves agreement between measured and modeled gas-particle partitioning for select major and minor components of the SOA, consistent with thermal decomposition during desorption causing the conversion of lower volatility components into the detected higher volatility compounds.

Published by Copernicus Publications on behalf of the European Geosciences Union.

1 Introduction

The sources, oxidation pathways, and chemical properties of secondary organic aerosol (SOA) remain highly uncertain on a molecular basis. These uncertainties can lead to large errors between modeled and measured aerosol loadings (Heald et al., 2010; Volkamer et al., 2006) and ultimately limit our ability to confidently predict changes in aerosol properties under a warming climate (Hallquist et al., 2009) or in response to other anthropogenic perturbations such as emissions of nitrogen oxides and sulfur dioxide. To develop adequate model parameterizations of organic aerosol (OA) formation, growth, and loss, there remains a need to improve and evaluate chemical mechanisms that involve conversion and partitioning of organic compounds between gas and condensed phases (Roldin et al., 2014). These needs are likely to be at least partially addressed by a more detailed understanding of molecular composition in both phases at higher time resolution from which mechanistic insights are more easily discerned.

While SOA is ubiquitous in the lower atmosphere, our understanding of its composition and properties, from nucleation and growth of freshly formed particles to background ambient particles, is still lacking (Donahue et al., 2011; Ehn et al., 2014; Riccobono et al., 2014; Riipinen et al., 2012; Ziemann, 2002). Identifying the sources and functional groups of organic molecules within SOA remains a difficult analytical challenge, given that their inherent low volatility makes routine online analysis by mass spectrometry impossible without perturbation (thermal desorption, dissolution, derivatization, etc.) and that the actual source molecules initially condensing into the particle phase may have been transformed via condensed phase chemistry, such as acid–base reactions or various organic accretion processes (Smith et al., 2010; Ziemann and Atkinson, 2012).

Recently, in situ measurement methods have been developed which can address the volatility distribution or molecular composition of organic aerosol. volatility tandem differential mobility analyzers allow the measurement of kinetic evaporation in a series of ovens, which can be used to constrain the bulk volatility of compounds present in the aerosol (Cappa, 2010). Similarly, thermal denuders have been coupled to aerosol mass spectrometers to examine the loss organic aerosol mass during transit through a programmatically heated oven with some molecular information derived from factor analysis (Cappa and Jimenez, 2010). Other chemically speciated measurements, for example the TAG (thermal desorption aerosol gas chromatograph) (Williams et al., 2006), measure the molecular composition of thermally desorbed compounds but lack a direct measure of the aerosol volatility and rather use functional group dependencies to infer the volatility distribution based on detected compositions. Holzinger et al. (2010) coupled an analogous collection-thermal-desorption inlet to a PTR-MS (proton transfer reaction mass spectrometer) to detect organic and inorganic compounds while also providing thermogram information, but this type of chemical ionization often leads to fragmentation and dehydration (Holzinger et al., 2010). We recently developed the FIGAERO (Filter Inlet for Gases and AEROsol), which allows both the separation of components in a volatility space, via a temperature-programmed thermal desorption, and the determination of the corresponding molecular composition on an hourly timescale (Lopez-Hilfiker et al., 2014).

We present measurements of compounds produced from α-pinene oxidation by OH and ozone in an environmental simulation chamber using the FIGAERO coupled to a high-resolution time-of-flight chemical ionization mass spectrometer (HR-ToF-CIMS) (Lopez-Hilfiker et al., 2014). Carboxylic acids are thought to be important components of monoterpene-derived SOA, in part because the acid functionality represents an approximate end point in carbon oxidation state and its incorporation leads to a significant reduction (1000 fold) in vapor pressure relative to the parent compound (Capouet and Müller, 2006; Russell et al., 2011). We therefore chose acetate negative proton transfer ionization, which is most sensitive to carboxylic acid groups (Veres et al., 2010, 2008) though it also detects other functionalities as we have previously demonstrated and extend herein (Mohr et al., 2013). Our main goal is not so much a functional group characterization but to examine the extent to which compounds containing acid functionalities contribute to the SOA and the distribution of these compounds in a volatility/abundance space. We find that a significant fraction of the SOA mass characterized by the HR-ToF-CIMS is of extremely low volatility, 4 or more orders of magnitude lower than typical monoterpene oxidation products. We discuss the implications of these compounds with respect to partitioning models and the lifetime of atmospheric aerosol.

2 Experimental methods

A prototype FIGAERO–HR-ToF-CIMS was coupled to both the Jülich Plant Atmosphere Chamber (JPAC), Jülich Forschungszentrum, Germany (Mentel et al., 2009), and a smaller chamber with similar conditions at the University of Washington (UW). Below we provide detailed descriptions of the coupling of the FIGAERO–HR-ToF-CIMS to the JPAC and UW chambers.

2.1 Simulation chambers

Most data presented here were obtained at the JPAC (Mentel et al., 2009), which consists of a series of glass chambers housed in separate temperature-controlled rooms. We used a 1450 L borosilicate glass chamber housed in a temperature-controlled room held at 15 °C and relative humidity (RH) of 35 to 65 %. The chamber is operated under steady-state conditions and is continuously stirred by a mixer mounted at the top of the chamber. The residence time is on average

50 min at a flush rate of ~ 30 standard L min^{-1}. The chamber is equipped with different types of UV lamps: one set can be used for photolysis of NO_2 to NO and the other set of lamps for OH production from O_3 photolysis in the presence of H_2O. The OH lamps can be shielded such that the actinic UV flux, and therefore the OH production rate, can be varied. We oxidized α-pinene with varying concentrations of O_3 and UV intensity, as well as in the presence and absence of effloresced ammonium sulfate seed particles, as part of a more extensive measurement campaign (PANDA – Probing Aerosol Nucleation During Alpha-pinene oxidation).

Here we present measurements at the end of the PANDA campaign when we utilized the FIGAERO inlet system. Concurrent measurements were made of gas-phase extremely low volatility organic compounds (ELVOC) (Ehn et al., 2014) using a nitrate CIMS (Jokinen et al., 2012), 1–3 nm sized particles with a particle size magnifier (Airmodus, Finland), the number size distribution from 3 to 600 nm using a scanning mobility particle sizer (SMPS, TSI model 3071), monoterpene concentrations using a quadrupole PTR-MS (Ionicon, Austria), and non-refractory particle composition with an high-resolution aerosol mass spectrometer (HR-AMS, Aerodyne, USA) (DeCarlo et al., 2006). We used the composition measured from the AMS and total particle volume from a SMPS to calculate particle mass of sulfate and SOA present in the chamber. The chamber was run in steady-state mode with constant addition of 30 ppb α-pinene and 80 ppb ozone. We began with α-pinene ozonolysis in the dark followed by OH oxidation, where the OH was produced by shielded UV lamps (Mentel et al., 2009). For both conditions, we added seed particles to increase the particle/chamber wall surface ratio in order to better compete with condensation and partitioning of low and semivolatile gases to the chamber walls (Matsunaga and Ziemann, 2010). We added effloresced (solid) ammonium sulfate particles with concentrations spanning from 0 to 70 µg m^{-3}. Except for the period at ~ 25 µg m^{-3} of sulfate, most seed particle concentrations were a momentary state, i.e., steady state was neither assessed nor likely achieved for most components.

A University of Washington chamber was also used for optimization and initial testing of the FIGAERO in steady-state conditions as well as batch mode experiments to explore the time dependence of oxidation products. The chamber consists of a 0.7 m^3 Teflon bag with multiple sampling or fill ports. The chamber is pressure controlled by a servo-controlled valve that regulates the draw of air out of the chamber held slightly above atmospheric pressure ($\sim +1$ mb). The chamber is continuously filled with zero air generated by a Teledyne zero air generator (Model 701) and flow is set by a 20 000 standard cm^3 min^{-1} mass flow controller (MKS 1179a). α-Pinene is delivered by a perforated Teflon diffusion tube held at room temperature or a vial of pure α-Pinene in an ice bath, the output from which mixes with the incoming zero air containing O_3 generated by passing 100 standard cm^3 min^{-1} of ultra-high purity (UHP) N_2 with 10 % O_2 through a UV photolysis cell. The α-pinene mass loading in the chamber is set by the ratio of flows through the diffusion source and the main chamber air. For the data discussed here, the RH of the UW chamber was < 5 %.

2.2 FIGAERO–HR-ToF-CIMS

The FIGAERO and its HR-ToF-CIMS coupling has been described in detail elsewhere (Lopez-Hilfiker et al., 2014), and therefore only a review of its general operation and differences from the standard operation is described here. The FIGAERO is essentially a multi-port inlet assembly that allows sampling of either gas-phase components or thermally desorbed particulate compounds into a high-resolution time of flight mass spectrometer (HR-ToF-CIMS) with selective detection by chemical ionization. Here we present results using acetate negative-ion proton transfer ionization (Veres et al., 2008). The instrument is continuously cycled between gas and particle analysis modes with periodic determinations of the particle and gas-phase background signals using a secondary filter (Lopez-Hilfiker et al., 2014).

A prototype of the FIGAERO–HR-ToF-CIMS was deployed at JPAC and installed directly under the chamber in the temperature-controlled chamber room. As the FIGAERO was primarily designed for ambient sampling at high flows, for faster particle concentration on the filter we reduced the flow rate across each of the inlets and changed the inlet tube diameters to be more appropriate for the low-flow conditions required on the chamber, which has a finite fill rate. At JPAC, chamber air was drawn at 10 standard L min^{-1} from the base of the chamber through a 1.5 m long 10 mm OD stainless steel tube. About 1 m of the tube extended into the center of the chamber, and the other 0.5 m spanned from the chamber edge to a manifold located at the instrument. Approximately 2 standard L min^{-1} was drawn from this manifold to sample the gas-phase composition via a 6.5 mm OD PTFE inlet with a length of approximately 12 cm to the HR-ToF-CIMS. Another 5 standard L min^{-1} was drawn from the manifold via a 20 cm length of 6.5 mm OD copper tube across the primary FIGAERO filter to collect particles. We collected particles for 30 min at 5 standard L min^{-1} and thermally desorbed the particles for 40 min at a ramp rate of 20 °C min^{-1} from ambient to 200 °C at which point the temperature was held constant to ensure that particle-phase signals returned to their pre-heating levels. The particle sample flow is monitored by a mass flow meter (MKS 1179a) to track the total volume sampled over the collection period and relates the integrated particle desorption signal area to a mass loading in the chamber.

To assess the particle background due to adsorption and/or absorption of gases onto the Teflon filter, we manually placed an identical filter in a Teflon filter holder immediately upstream of the FIGAERO filter. Particle backgrounds were conducted at each photochemical condition in the chamber,

usually multiple times, to obtain representative backgrounds at each stage. Gas-phase backgrounds were assessed at the point prior to desorption when the instrument is sampling UHP N_2 and also when the pre-filter was in place, which allows for assessing whether particle components volatilized in the heated portions of the ion–molecule reaction (IMR) and transfer tubing between the prototype FIGAERO filter and the IMR.

2.3 Acetate chemical ionization

The measurements reported here were obtained using acetate ionization, employed as described previously (Mohr et al., 2013; Veres et al., 2008; Yatavelli et al., 2012). The dominant ionization mechanism is expected to be proton abstraction governed by the gas-phase pK_a of a compound relative to acetic acid.

$$\mathrm{HA} + \mathrm{CH_3C(O)O^-(CH_3C(O)OH)}_n \rightarrow \mathrm{A^-(CH_3C(O)OH)}_n + \mathrm{CH_3C(O)OH} \quad \text{(R1)}$$

The reagent ion cluster distribution is unknown for our conditions, but tests changing the collisional declustering after the ionization region indicate $n = 1$ with some minor contribution from $n = 2$ or higher. The collisional declustering strength is set such that $\sim 99\,\%$ of the reagent ion is detected as $n = 0$ and $< 1\,\%$ is detected as $n = 1$ or higher. Thus, ion-neutral clusters are likely to be minor components of the ion signal. The sensitivity of the instrument was periodically calibrated during the JPAC campaign by adding the output of a formic acid permeation device to the inlet. The permeation device output was calibrated gravimetrically before and after the measurements.

The acetate chemical ionization scheme is still relatively novel, and as such its selectivity and sensitivity towards a large range of compounds and functional groups remains to be characterized. For this reason, we performed a series of calibrations after the measurement campaign to investigate the sensitivity of acetate ionization to a series of carboxylic acids, RC(O)OH, and related functional groups, such as peroxy acids, RC(O)O–OH, and a diacyl peroxide (benzoyl peroxide) (see Fig. 1). In all cases, compounds were calibrated as described previously (Mohr et al., 2013). For these tests, the walls of the IMR region were heated to 60 °C – though it is unlikely the gas equilibrates to that temperature for the ~ 100 ms of transit through the region. While limited in number and type, the compounds tested to date suggest that acetate ionization, as employed in our instrument, converts peroxy acids to the corresponding carboxylate anion with nearly the same efficiency as the corresponding carboxylic acids. In addition, benzoyl peroxide is detected at the benzoate anion more efficiently than is benzoic acid. Other functional groups, e.g., polyols and esters, were not detected nearly as efficiently, nor were clusters of the tested components with acetate ions detected at significant signals. Thus we conclude, perhaps conservatively, that acetate ionization is a measure of functionalities that can easily produce carboxylate anions, such as peroxy acids and diacyl peroxides in addition to carboxylic acids under the operating conditions used here.

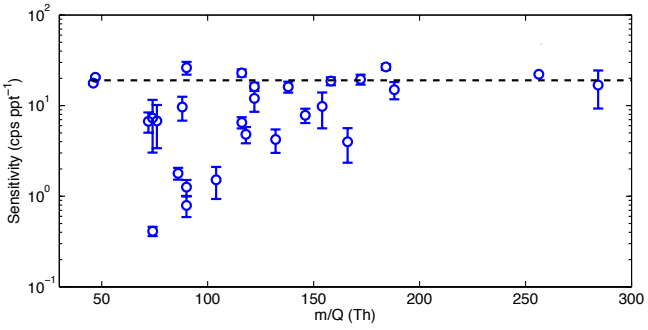

Figure 1. The distribution of observed sensitivities to carboxylic acids using acetate reagent ions. Error bars are 1σ based on multiple injections of solutions following Mohr et al. (2013). The black dashed line shows the sensitivity value used for bulk analysis.

For compounds with a carboxyl-related group, there appears to be a convergence of sensitivity towards a maximum value similar to that for formic acid (see Fig. 1). Given the available evidence, using this maximum sensitivity value for the entire spectrum would presumably lead to a lower-limit estimate of the mass concentrations of such compounds in the chamber. Clearly, further investigation and optimization of acetate ionization selectivity is needed, as is care attributing any signal to a specific functionality measured with acetate ionization. That said, our main conclusions are not dependent upon the exact functional groups acetate detects.

3 Results

3.1 Contribution of acyl-containing compounds to α-pinene SOA

Figure 2 shows an overview of the key aerosol measurements during the time when the FIGAERO was installed at JPAC. As the surface area concentration of the seed particles increased, the detected AMS organic aerosol mass increased while the amount of monoterpene reacted remained constant. Consequently, during ozonolysis conditions, the inferred SOA mass yield increased from 1 to 10 % even though the α-pinene reacted remained constant. Similarly, the inferred SOA mass yield nearly doubled during OH oxidation of constant $\Delta(\alpha\text{-pinene})$ just by adding seed particles. The absolute abundance of detected compounds in the particle phase, measured by the FIGAERO, also increases with the addition of seed and is highly correlated with the total SOA measured by the AMS at all times. However, the fractional contribution of "acyl-containing" compounds to SOA changes little over the varying SOA mass concentration and oxidant conditions (inset Fig. 2).

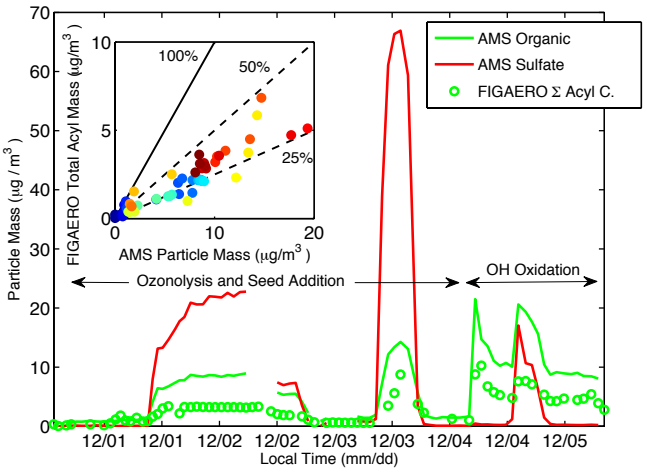

Figure 2. An overview of the experiments conducted in the JPAC chamber. Green and red lines are total organic and sulfate mass concentrations measured by an HR-AMS. The total organic aerosol mass detected by the AMS responded to changes in seed concentrations, increasing the inferred SOA yield. Size selected ammonium sulfate additions were performed to increase the particle surface area relative to chamber walls. The sum FIGAERO–HR-ToF-CIMS particulate mass using acetate reagent ions is shown in green circles using the formic acid sensitivity for all detected compositions (see text for details). Inset: correlation between the HR-AMS-derived total organic aerosol mass concentrations and the FIGAERO–HR-ToF-CIMS-derived total "acyl"-containing compound mass concentrations shows that across all chamber conditions the FIGAERO measurements explain 25–50 % of the total organic aerosol mass.

To make the comparison between the FIGAERO–HR-ToF-CIMS and AMS quantitative, we used the sensitivity of the instrument to formic acid (ions s^{-1} $mole^{-1}$ m^{-3}) as a measure of the average sensitivity to all detected compounds. Based on the data shown in Fig. 1, this assumption is reasonable to within a factor of 1.5 as governed by the spread of calibration factors to individual compounds, especially in the m / Q range where much of the particle-phase mass is detected. We include in the analysis only ions having a molecular formula ($C_xH_yO_z$) that contain at least 1 degree of unsaturation, an odd number of H atoms, and at least two O atoms. This selection represents the vast majority of signal measured during these experiments (> 85 %). We convert the integrated thermograms of each ion to μg m^{-3} using the formic acid sensitivity, the molecular mass of the ion plus the mass of one H, and the volume of air sampled prior to the thermogram measurement (see Lopez-Hilfiker, et al., 2014, for more details). The resulting total signal accounts for 25–50 % of the organic aerosol measured by the AMS. We discuss the volatility distribution and phase partitioning of this significant fraction of OA below.

3.2 Gas-particle partitioning: measurement, theory, and the role of thermal decomposition

As the FIGAERO allows measurement of compounds in both the gas and particle phase, we are able to assess the phase partitioning directly of individual molecular compositions, after accounting for the volumetric concentration in the particle-phase inlet relative to the instantaneous gas-phase measurement. To calculate the phase partitioning, we follow a similar procedure to that of Yatavelli et al. (2014), defining fraction in the particle phase (F_p) as the concentration in the particle phase divided by the sum of gas and particle phases (Eq. 1) for a given ion elemental composition. Because the HR-ToF-CIMS does not resolve structural isomers, this approach implicitly assumes that all isomers with the same elemental composition have the same saturation vapor pressures and activity coefficients. Before evaluating phase partitioning, we first assess this assumption by performing an analysis of the thermal desorption profiles, i.e., "thermograms", for specific ion compositions.

In Fig. 3 (top panels), we show the thermal desorption profiles for two molecular compositions, $C_8H_{12}O_4$ (left) and $C_9H_{14}O_4$ (right), consistently measured as major components of the detected monoterpene SOA. For the purposes of comparing to a phase partitioning model below, we assume these compositions represent common pinene-derived acids – pinic and norpinic acid, though terpenylic acid (Yasmeen et al., 2010) is also a possibility for the latter. As shown in our previous work (Lopez-Hilfiker et al., 2014), thermograms of compounds desorbing from synthetic mixtures deposited on the filter exhibit fairly uniform single-mode desorption profiles, with signal maxima occurring at distinct desorption temperatures which correlate with a compound's enthalpy of sublimation. In contrast, the multi-modal form of the thermograms of individual α-pinene SOA components suggests these thermograms contain added chemical information about either the presence of isomers with vastly different heats of vaporization (vapor pressures) or higher molecular mass and lower volatility compounds that thermally decompose into the compositions which are measured by the HR-ToF-CIMS.

To further investigate the sources of, and thus information carried by, the more complex desorption features observed in the α-pinene SOA (shoulders, multiple modes, enhanced tailing, etc), we applied a custom nonlinear least squares peak-fitting routine to the thermograms. First, single-mode thermogram peaks are identified and standardized on a normalized width scale. The resulting normalized peaks are averaged to obtain a typical thermogram peak shape that represents the desorption profile of a single component. An iterative routine using the Levenberg–Marquardt algorithm for nonlinear least squares problems fits the multimodal thermograms by applying a variable number of thermogram peaks having the average desorption peak shape. The number, location, and amplitude of each additional desorption peak within

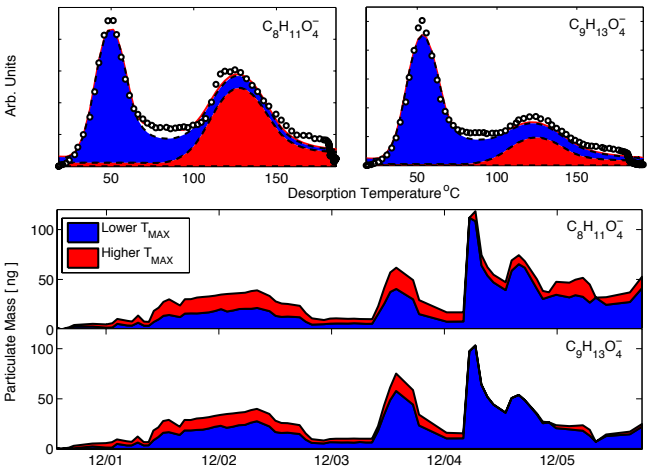

Figure 3. Top panels: thermograms for two ion compositions, each showing two distinct modes in the thermogram, are plotted showing the results of fitting desorption profiles characteristic of an individual compound with a specific enthalpy of sublimation. The first, lower temperature, modes are consistent with the corresponding carboxylic acid desorbing as a non-interacting component of the collected organic aerosol. We attribute the second, higher temperature modes, to thermal decomposition of lower volatility compounds (such as oligomers or highly functionalized monomers) which are thermally unstable and which presumably do not affect the partitioning of the primary acids between the gas and particle phases. Lower Panels: the time series of the individual peak integrations within a fitted thermogram for the two different ion compositions across all chamber conditions. A significant fraction of the total detected signal arises from thermal decomposition (red) during desorption. Evident is the nearly complete disappearance of the second mode in $C_9H_{13}O_4^-$ (pinic acid) during OH oxidation, suggesting that it is derived from a precursor that is only present during ozonolysis or which is reacted away in the presence of OH.

a thermogram are optimized to explain the total thermogram of a given ion. To allow for individual compounds having slightly different desorption profiles, the width of the typical desorption peak shape is allowed to vary by up to 30 % based on fitting a range of thermograms from pure component desorption.

Typical results from this thermogram-fitting routine are shown in the top panels of Fig. 3. Two or three separate particle-phase components are desorbing as $C_8H_{12}O_4$ ("norpinic") and $C_9H_{14}O_4$ ("pinic") at distinctly different temperatures. Blue areas represent the fraction of the detected mass desorbing at lower temperatures and which would be consistent with desorption temperatures expected for norpinic or pinic acid volatilities based on our relationship between enthalpy of sublimation (vapor pressure) and desorption temperature (Lopez-Hilfiker et al., 2014). In red, we show the contribution of secondary modes to the overall thermogram that occur at much higher temperatures than expected for these compounds. There is a third possible intermediate bin, but its presence is always much smaller and not statistically significant across the full time series, and so it is not included in the time series discussed below. Based on our calibrated desorption-temperature axis, the two major portions of the thermograms correspond to order-of-magnitude effective 298 K saturation vapor pressures of $\sim 10^{-4}$, and $\sim 10^{-10}$ Pa (or C^* of ~ 10 and $\sim 10^{-6}$ µg m^{-3}). As it is highly unlikely that there would be two structural isomers (one for norpinic and one for pinic acid) with vapor pressures 6 orders of magnitude lower than the other isomers, we conclude that the secondary desorption events are caused by larger molecular weight compounds, e.g., oligomeric accretion reaction products, thermally decomposing to compounds with the same compositions as norpinic and pinic acid that subsequently desorb and are detected by the HR-ToF-CIMS. Large macromolecules are of sufficiently low volatility that the enthalpy of vaporization is very likely larger than the dissociation energies of their weakest bonds, leading to preferential decomposition into smaller components (e.g., oligomeric building blocks) instead of evaporation. For example, we note here that a typical O–O bond energy (one of the weaker organic covalent bonds) is ~ 140 kJ mol^{-1} (Blanksby and Ellison, 2003; Epstein et al., 2010), which corresponds to a desorption temperature of ~ 80°C based on our calibration of sublimation enthalpy, though other thermal decomposition processes are of course possible. This idea is consistent with previous work using a temperature-programmed thermal desorption which also investigated the multimodal nature of thermally desorbed SOA from the reaction of a-pinene and ozone (Docherty et al., 2005), which concluded a large fraction of the SOA formed consisted of organic peroxides.

In the bottom panels of Fig. 3 we show the time series of the fractional contribution each of the fitted desorption peaks makes to the overall thermogram area. Interestingly, the lower volatility secondary modes in the thermal desorption of norpinic and pinic acids are more prominent during ozonolysis than OH-dominated oxidation of α-pinene. Despite increased overall production (mass loading) of pinic and norpinic acids during OH-dominated oxidation, the secondary modes are much less important, especially in the pinic acid case. Aside from providing a potential mechanistic insight into the chemical origins of these lower volatility compounds, their varying importance due to a change only in the chamber photochemical conditions suggests that these secondary modes are likely not an artifact of the desorption process but rather are evidence for lower volatility components that decompose into the C_8 and C_9 acids.

With the above insights into the thermal desorption process, we can more accurately assess gas-particle partitioning. We use equilibrium partitioning theory first described by Pankow (1994) to model the phase partitioning of three monoterpene-derived acids: pinic, norpinic, and pinonic acids. Equation (2) shows the transformation of equilibrium partitioning theory to a formulation of fraction in the particle phase (F_p) that we use to evaluate the quality of agreement

between modeled and measured partitioning.

$$F_{\mathrm{p}} = \frac{\mathrm{Particle}}{\mathrm{Gas} + \mathrm{Particle}} \quad (1)$$

$$F_{\mathrm{p}} = \left(1 + \frac{\frac{M 10^6 \zeta P}{760 RT}}{C_{\mathrm{OA}}}\right)^{-1} \quad (2)$$

In Eq. (2), C_{OA} ($\mu g\,m^{-3}$) is the organic aerosol mass concentration, M ($g\,mol^{-1}$) is the molar mass of the compound of interest, ζ is the activity coefficient, which we assume is unity (and discuss later in detail), P (torr) is the vapor pressure of compound the over the pure component, R ($8.2 \times 10^{-5}\,m^3\,atm\,K^{-1}\,mol^{-1}$) is the gas constant, T (K) is the environmental temperature, and 760 ($torr\,atm^{-1}$) and 10^6 ($\mu g\,g^{-1}$) are unit conversion factors. As the JPAC chamber is held at fixed temperature (15 °C), the free variables in Eq. (2) become the total organic mass concentration, which was measured by the AMS and SMPS, and the pure compound saturation vapor pressure. Using literature values to constrain saturation vapor pressures, specifically those predicted by the structure activity relationship of Capouet and Müller (2006), we then evaluate whether or not equilibrium adsorptive partitioning explains the observed phase partitioning for our chamber conditions (Capouet and Müller, 2006).

Based on the thermogram analysis presented above, it is highly unlikely that norpinic and pinic acid partitioning would be well described by an equilibrium partitioning model that assumed all of the measured particle mass (thermogram area) carried in those two acids was in equilibrium with the corresponding gas-phase acids. We demonstrate this issue in Fig. 4. In the top panels of Fig. 4, we show the thermal desorption profiles for the three molecular compositions, $C_9H_{14}O_4$, $C_{10}H_{16}O_3$, and $C_8H_{12}O_4$, from particles collected under each set of conditions (O_3+ seed and OH). Ozonolysis conditions are shown in black, while OH oxidation conditions are shown in red. As above, we assume these compositions correspond to pinic, pinonic acid, and norpinic acids, respectively. Pinonic acid provides a useful contrast to the other two in that it does not show evidence for secondary desorption peaks under either set of conditions.

Previous comparisons to adsorptive partitioning models have used the full integrated thermogram arising from thermal desorption to compare with the model prediction and found varying levels of agreement (Yatavelli et al., 2014; Zhao et al., 2013). In the middle panels of Fig. 4, we plot the measured F_{p}, calculated from the full integral of the thermogram, versus the F_{p} predicted by the adsorptive partitioning model. The points are colored by experiment time, with reddish points corresponding to OH oxidation towards the end of the experiment and all other colors (blueish) corresponding to ozonolysis conditions. Generally poor agreement is observed, highlighted by nonlinearity and by points falling far from the 1 : 1 line. There is one exception: pinic acid during OH oxidation (red points). This condition is also when

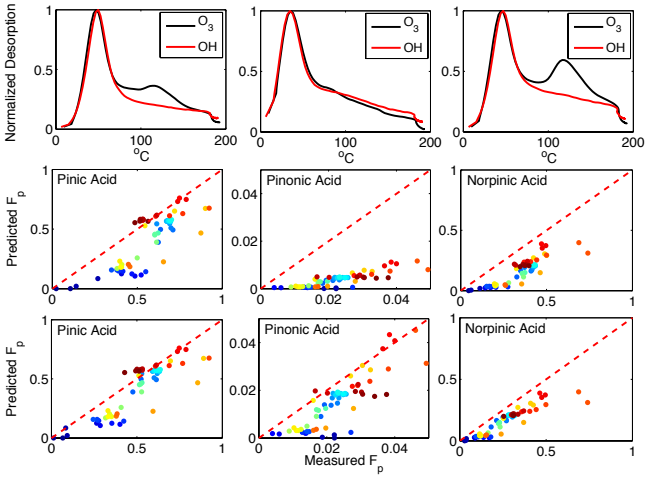

Figure 4. Top panels: thermogram shapes for ozonolysis conditions (black) and OH oxidation (red) for the ion compositions corresponding to those of pinic, pinonic, and norpinic acids (left to right). Middle panels: comparison between modeled and measured gas-particle partitioning (F_{p}). Generally poor agreement is found with nonlinearity and points far from the 1 : 1 line (red dashed). Bottom: the same partitioning comparison but with the thermogram-fitting routine (Fig. 3) applied to remove the secondary modes in the desorption profile which are likely a result of thermal decomposition (see text for details). For pinonic acid a single desorption mode is observed under all conditions. To achieve model measurement agreement an activity coefficient of 0.25 is required, or the pure compound vapor pressure used is too high by a factor of ~ 4.

the thermogram for the composition corresponding to pinic acid is largely a single mode (see Fig. 4, top), suggesting that if the thermograms are deconvolved into contributions representing the different modes, the agreement between measured and predicted F_{p} would improve.

In the lower panels of Fig. 4 we show the results of deconvolving the thermograms into the different modes using the above fitting approach for a more direct test of the actual partitioning of these three acids into the particle phase. Based on our previous work, compounds with compositions similar to those under consideration here, C_8–C_{10} keto and diacids, would have thermogram signals that maximize at a desorption temperature (T_{max}) of 80 °C, or below, if they were non-interacting components of a solution (Lopez-Hilfiker et al., 2014). Therefore, in our revised partitioning analysis we assume that in order to be in dynamic equilibrium with the gas-phase, a compound should desorb from the particle phase at a temperature consistent with its expected enthalpy of sublimation. Thus, we use only a portion of the area under the thermogram to calculate the particle-phase concentration of each acid in equilibrium with that in the gas phase. In this case, that area corresponds to the desorption mode at the lowest temperature in the thermogram analysis. The other peaks and shoulders in the thermograms that arise at significantly higher temperatures are presumably from processes

related to thermal decomposition and/or high-temperature formation of acid functionalities which produce the molecular "fragments" detected by the CIMS. The abundance of these molecular "fragments" from lower volatility components would have no direct impact on the equilibrium partitioning of the actual C_8–C_{10} acids. Accounting for these structures in the thermograms leads to much better agreement (pinic acid: $R^2 = 0.8$, slope = 0.99, intercept −0.07; norpinic acid: $R^2 = 0.92$, slope = 0.78, intercept −0.04) between the partitioning model and measured F_p for pinic and norpinic acids across all chamber conditions, suggesting that (i) literature estimates of their saturation vapor pressures used herein are reasonable, that (ii) partitioning based on Raoult's law is applicable under the chamber conditions, and therefore that (iii) particle viscosities cannot be so high as to disrupt the equilibration process on the ∼ hour timescale of the chamber measurements.

The revised partitioning calculation, using the thermogram-fitting approach, does not improve the measurement–model agreement for pinonic acid. Pinonic acid desorbs as a single peak under all conditions, therefore providing no basis for selecting a smaller portion of the thermogram area. Yet, pinonic acid clearly desorbs from the α-pinene SOA at a temperature ($T_{max} \sim 40\,^{\circ}C$) that is significantly higher than if placed on the filter in pure form (or part of a synthetic mixture), where it desorbs at $T_{max} << 32\,^{\circ}C$ (Lopez-Hilfiker et al., 2014). Our measurements therefore suggest that the effective vapor pressure of pinonic acid is lowered over the SOA ($F_p^{measured} >> F_p^{predicted}$) relative to over the pure substance or an ideal solution. As the temperature of maximum desorption for pinonic acid from the α-pinene SOA is less than that required to break the weakest of covalent bonds, and because the thermogram is a single mode, it is unlikely that the pinonic acid desorption arises from the same processes that we hypothesize give rise to the secondary peaks in the thermograms of pinic and norpinic acids. We note that there are potentially lower energy pathways to decomposition than a typical bond strength analysis might suggest, and therefore decomposition cannot easily be ruled out. However, the measurement–model agreement is highly linear, suggesting a single adjustment in the pinonic acid vapor pressure, i.e., an activity coefficient different from unity (∼ 0.25), would bring agreement under most conditions (see Fig. 4, bottom). Enhanced H bonding of pinonic acid in the multi-functional SOA environment relative to the pure substance could explain these behaviors.

We conclude this section by noting that thermal decomposition of particulate organic material likely occurs in any technique that utilizes heat to drive compounds into the gas phase for analysis. However, by utilizing a calibrated relationship between molecular composition and desorption temperature, together with a slow desorption-temperature ramp rate, the effects of thermal decomposition on inferred vapor-pressure-driven partitioning can be addressed and even utilized to arrive at a more complete view of SOA composition and volatility as we demonstrate below.

3.3 Bulk aerosol volatility

Above we provided specific examples of how a consistent framework can be used to relate SOA molecular composition and vapor-pressure-driven partitioning to thermal desorption measurements. However, as shown in Fig. 5 (top), we observe many (hundreds) of compounds which desorb at much higher temperatures from α-pinene ozonolysis SOA than consistent with their composition. These particular data were obtained from analyzing α-pinene ozonolysis SOA generated in the UW chamber under steady-state continuous-flow conditions. The points are sized by the square root (for dynamic range) of the particle mass concentration for each molecular composition detected and colored by its thermogram T_{max}. A swath of compounds containing one to five carbon atoms all desorb at temperatures between 50 and 90 °C, similar to much lower volatility compounds such as C_8–C_{10} diacids and certainly inconsistent with expected heats of vaporization for those small compounds. We hypothesize that this whole group of compounds (light blue) results from decomposition of larger molecules or from weakly bound complexes that effectively lower the vapor pressures of these smaller compounds.

The simplest way to organize and reduce the information in Fig. 5 (top) is by summing the calibration adjusted signal across all detected compounds. We show an example of the resulting sum thermogram in Fig. 5 (bottom). Using the thermogram-fitting approach discussed above, as well as our previously determined volatility axis based on desorption temperature, we can examine the bulk volatility of the α-pinene ozonolysis SOA detected by the FIGAERO–HR-ToF-CIMS from the sum thermogram. We find that three volatility modes are required to explain the sum thermogram. The first mode is centered at ∼ 60 °C, consistent with volatilities of C_8–C_{10} diacids ($C^* \sim 1$–$10\,\mu g\,m^{-3}$). This mode represents ∼ 50 % of the measured desorption signal. Two other modes are apparent at higher desorption temperatures, one maximizing at ∼ 110 °C and the other at ∼ 150 °C. Clearly, a large fraction of the total mass of detected compounds desorbing from the α-pinene SOA are from very low volatility components. In the upper panel of Fig. 5, these higher temperature modes correspond to the appearance of C_{15}–C_{20} compounds, lending support to the conclusion that large molecular weight accretion products are a source of the smaller molecular components that also maximize at higher temperatures. Roughly 50 % of the signal measured during a desorption occurs at temperatures greater than 100 °C, corresponding to effective $C^* < 10^{-5}\,\mu g\,m^{-3}$.

The above estimates of C^* values and carbon mass associated with them are probably upper and lower limits, respectively, because extremely low volatility compounds likely decompose before desorbing, which biases the measured

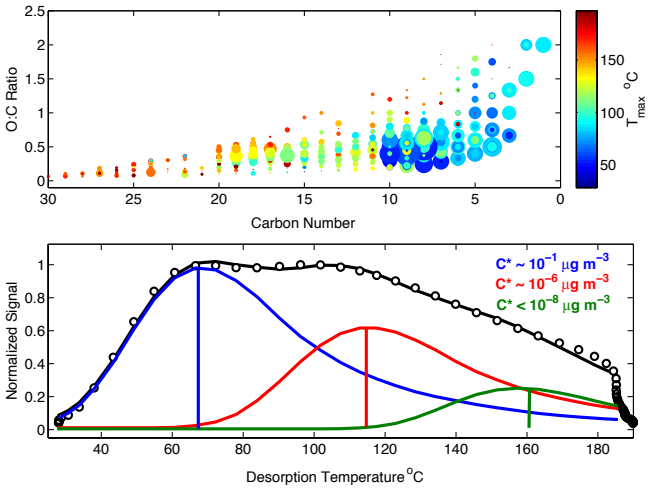

Figure 5. Top: points are plotted sized by the square root of their particle-phase desorption signal. Evident is a secondary mode in abundance space between carbon number 15 and 20. Each compound is colored by the temperature of maximum desorption signal, which is related to a compound's enthalpy of sublimation (saturation vapor pressure) as shown previously (Lopez-Hilfiker et al., 2014). Bottom: a sum thermogram, i.e., the entire mass spectral signal at each measurement time (using selection criteria detailed in the text), is summed and plotted versus desorption temperature. Clearly SOA from α-pinene ozonolysis exhibits multiple modes. The first mode is consistent with monoterpene-derived diacids, whereas the secondary modes which arise at temperatures > 100 °C have effective vapor pressures at least 4 orders of magnitude lower than common monoterpene oxidation products.

volatility higher, and the acetate ionization scheme may not be sensitive to all of the decomposition fragments, which biases the detected mass lower.

4 Discussion

From an analysis of molecular thermograms of α-pinene SOA generated in chambers, we find that a large fraction of the characterized SOA is of very low volatility, with compositions having > 10 C, and > 4 O. Moreover, we find that acetate ionization can explain at least 25–50 % of the total SOA. We conclude that large molecular weight compounds must be present in the aerosol. Indeed, we directly observe compounds with up to as many as 30 carbon atoms and up to 10 oxygen atoms desorbing from the α-pinene SOA. Additional indirect evidence is that commonly reported oxidation products of α-pinene, such as pinic, norpinic, and other carboxylic acids desorb at temperatures far too high to be consistent with their expected enthalpies of vaporization. Treating all of the mass that desorbs from the particles in the form of these common and smaller products as being in vapor-pressure-driven equilibrium with the corresponding gas-phase compounds leads to large errors between modeled and measured gas-particle partitioning that cannot be explained by a simple adjustment of the saturation vapor concentration or its temperature dependence. Moreover, that some 50 % or more of the CIMS-detected SOA mass is effectively nonvolatile, having $C^* < 10^{-5}$ µg m^{-3}, conflicts with previous conclusions that α-pinene ozonolysis SOA is predominantly semivolatile (An et al., 2007; Hallquist et al., 2009) but could be consistent with recent evidence that α-pinene SOA might be semisolid (Renbaum-Wolff et al., 2013).

Our findings are broadly similar with other online and offline molecular characterizations of α-pinene SOA, which have found evidence for oligomeric compounds (DePalma et al., 2013; Gao et al., 2004; Hall and Johnston, 2011, 2012). Our approach combines slow temperature ramps and molecular characterization without chromatography and thus provides a compliment to methods that have observed oligomeric material using liquid extraction followed by chromatography and electrospray ionization or particle beam thermal desorption coupled to electron impact ionization (Ziemann, 2002). We provide an additional constraint on the fraction of SOA that is contained in these oligomeric compounds and how that fraction varies in response to different photochemical regimes.

The addition of OH and UV light suppresses the secondary low volatility modes in the thermograms of pinic and norpinic acids, which suggests that the products formed via accretion chemistry may be susceptible to photolysis and reaction with OH or involve a precursor formed only during ozonolysis. The presence of peroxides as macromolecule linkages is certainly consistent with our results given that the secondary modes in thermograms of many compounds arise at temperatures above the O–O bond strength, the weakest covalent bond. That there might be a significant source of low-volatility peroxide compounds in α-pinene SOA was shown recently by Ehn et al. (2014). Whether the oligomeric compounds we observe are from $RO_2 + RO_2$ reactions in the gas-phase or from particle-phase accretion reactions such as peroxy hemiacetal formation, or some combination thereof, is beyond the scope of this paper but should be addressed in future studies in order to more accurately represent their contribution to SOA in models (Docherty et al., 2005; Ziemann and Atkinson, 2012).

We use an estimate of the O–O bond strength to put desorption temperature into a chemical bond context, but the O–O bond strength will depend upon molecular structure, and thus there is likely a distribution across the desorption-temperature space of molecular fragments desorbing at higher temperatures than their composition would suggest due to O–O bond cleavage. Additionally, there may be other bond scission pathways beyond the O–O functionality which we have not yet identified. The pinonic acid thermogram is a possible example, desorbing from the α-pinene SOA at temperatures well below the O–O bond strength equivalent but well above that expected from its known enthalpy of vapor-

ization. Non-covalent H bonding within the SOA matrix that is stronger or more ubiquitous than in pure single component samples or simple ideal mixtures is another mechanism to explain lower-than-expected volatility. Three persistent H bonds would be equivalent to about half the bond strength of an O–O bond (Dougherty, 1998). Oligomeric material may also be in thermodynamic equilibrium with semivolatile material such that losses of semivolatile compounds even at temperatures lower than the weakest covalent or hydrogen bond could lead to decomposition of oligomeric material to reachieve equilibrium. Processes like these need not occur at high temperatures but also may occur at near-ambient temperatures. The FIGAERO approach would potentially be able to capture this process if the evaporation rate of monomers was large enough to produce detectable signal prior to ramping the temperature of the desorption N_2. That said, a majority of detected SOA mass desorbed at temperatures well above covalent bond strengths.

Previous studies to characterize the molecular composition and partitioning of atmospheric aerosol have observed small-oxygenated organics that were present in larger-than-expected concentrations based on ideal partitioning. We show thermal decomposition of large molecules can be a significant bias in thermal desorption techniques, resulting in smaller stable fragments that are then detected. The process of thermal decomposition is likely common to any instrument which uses heat to drive aerosol components into the gas phase for analysis (Holzinger et al., 2010; Smith et al., 2010; Williams et al., 2006; Yatavelli et al., 2012; Zhao et al., 2013). Our measurements utilizing the FIGAERO indicate that "small acids" present in higher than expected concentrations in SOA are likely entirely due to thermal decomposition of much lower volatility components of the aerosol.

5 Conclusions

We have explored the contribution, composition, and volatility of acyl-containing organic compounds present in α-pinene-derived secondary organic aerosol under atmospherically relevant conditions using the FIGAERO–HR-ToF-CIMS. The distribution of detected compounds spanned $C_{1–30}$ and $O_{2–10}$ with many of the compounds that were detected in the gas phase also present in the particle phase. The distribution of acyl-containing compounds in the particle phase explains at least 25 % of the total SOA mass produced under both OH oxidation and ozonolysis conditions and shows evidence of a significant contribution from oligomers and other large macromolecules, especially during ozonolysis. The volatility of the detected mass reflects this contribution, with a large fraction of the organic mass having vapor pressures 4 orders of magnitude lower than commonly detected diacid products from ozonolysis of α-pinene. In the particle analysis we highlight the role of thermal decomposition and show that, when it is accounted for using the thermogram desorption profiles, equilibrium absorptive partitioning explains well the observed phase partitioning of pinic and norpinic acids though a non-ideal activity coefficient is required for pinonic acid under all conditions.

That we infer a significant fraction of the SOA is comprised of oligomeric compounds given the relatively short residence times of the JPAC and UW chambers (45–60 min) and the relatively small amount of α-pinene reacted in each case ($\sim$ 10 ppb), suggests these types of compounds can play an important role in ambient monoterpene-derived SOA. If that is the case, it would imply that a significant fraction ($\sim$ 25 % or perhaps more) of monoterpene ozonolysis SOA should be treated as effectively nonvolatile in atmospheric models. Future work utilizing the FIGAERO in the field will allow analysis of ambient aerosol for comparison, thereby providing a consistent view of SOA volatility and composition that will provide a direct test of these conclusions.

Acknowledgements. We would like to thank the supporting staff and scientists at the Jülich Research Facility. This work was supported by the US Department of Energy through awards from the Atmospheric System Research (DOE Grant DE-SC0006867) and SBIR (DE-SC0004577) programs.

Edited by: A. Nenes

References

An, W. J., Pathak, R. K., Lee, B.-H., and Pandis, S. N.: Aerosol volatility measurement using an improved thermodenuder: Application to secondary organic aerosol, J. Aerosol Sci., 38, 305–314, doi:10.1016/j.jaerosci.2006.12.002, 2007.

Blanksby, S. J. and Ellison, G. B.: Bond Dissociation Energies of Organic Molecules, Acc. Chem. Res., 36, 255–263, doi:10.1021/ar020230d, 2003.

Capouet, M. and Müller, J.-F.: A group contribution method for estimating the vapour pressures of α-pinene oxidation products, Atmos. Chem. Phys., 6, 1455–1467, doi:10.5194/acp-6-1455-2006, 2006.

Cappa, C. D.: A model of aerosol evaporation kinetics in a thermodenuder, Atmos. Meas. Tech., 3, 579–592, doi:10.5194/amt-3-579-2010, 2010.

Cappa, C. D. and Jimenez, J. L.: Quantitative estimates of the volatility of ambient organic aerosol, Atmos. Chem. Phys., 10, 5409–5424, doi:10.5194/acp-10-5409-2010, 2010.

DeCarlo, P. F., Kimmel, J. R., Trimborn, A., Northway, M. J., Jayne, J. T., Aiken, A. C., Gonin, M., Fuhrer, K., Horvath, T., Docherty, K. S., Worsnop, D. R., and Jimenez, J. L.: Field-Deployable, High-Resolution, Time-of-Flight Aerosol Mass Spectrometer, Anal. Chem., 78, 8281–8289, doi:10.1021/ac061249n, 2006.

DePalma, J. W., Horan, A. J., Hall IV, W. A., and Johnston, M. V.: Thermodynamics of oligomer formation: implications for secondary organic aerosol formation and reactivity, Phys. Chem. Chem. Phys., 15, 6935, doi:10.1039/c3cp44586k, 2013.

Docherty, K. S., Wu, W., Lim, Y. B., and Ziemann, P. J.: Contributions of Organic Peroxides to Secondary Aerosol Formed from

Reactions of Monoterpenes with O_3, Environ. Sci. Technol., 39, 4049–4059, doi:10.1021/es050228s, 2005.

Donahue, N. M., Epstein, S. A., Pandis, S. N., and Robinson, A. L.: A two-dimensional volatility basis set: 1. organic-aerosol mixing thermodynamics, Atmos. Chem. Phys., 11, 3303–3318, doi:10.5194/acp-11-3303-2011, 2011.

Dougherty, R. C.: Temperature and pressure dependence of hydrogen bond strength: A perturbation molecular orbital approach, J. Chem. Phys., 109, 7372, doi:10.1063/1.477343, 1998.

Ehn, M., Thornton, J. A., Kleist, E., Sipilä, M., Junninen, H., Pullinen, I., Springer, M., Rubach, F., Tillmann, R., Lee, B., Lopez-Hilfiker, F., Andres, S., Acir, I.-H., Rissanen, M., Jokinen, T., Schobesberger, S., Kangasluoma, J., Kontkanen, J., Nieminen, T., Kurtén, T., Nielsen, L. B., Jørgensen, S., Kjaergaard, H. G., Canagaratna, M., Maso, M. D., Berndt, T., Petäjä, T., Wahner, A., Kerminen, V.-M., Kulmala, M., Worsnop, D. R., Wildt, J., and Mentel, T. F.: A large source of low-volatility secondary organic aerosol, Nature, 506, 476–479, doi:10.1038/nature13032, 2014.

Epstein, S. A., Riipinen, I., and Donahue, N. M.: A Semiempirical Correlation between Enthalpy of Vaporization and Saturation Concentration for Organic Aerosol, Environ. Sci. Technol., 44, 743–748, doi:10.1021/es902497z, 2010.

Gao, S., Keywood, M., Ng, N. L., Surratt, J., Varutbangkul, V., Bahreini, R., Flagan, R. C., and Seinfeld, J. H.: Low-Molecular-Weight and Oligomeric Components in Secondary Organic Aerosol from the Ozonolysis of Cycloalkenes and α-Pinene, J. Phys. Chem. A, 108, 10147–10164, doi:10.1021/jp047466e, 2004.

Hall IV, W. A., and Johnston, M. V.: Oligomer Content of α-Pinene Secondary Organic Aerosol, Aerosol Sci. Tech., 45, 37–45, doi:10.1080/02786826.2010.517580, 2011.

Hall IV, W. A., and Johnston, M. V.: The Thermal-Stability of Oligomers in Alpha-Pinene Secondary Organic Aerosol, Aerosol Sci. Tech., 46, 983–989, doi:10.1080/02786826.2012.685114, 2012.

Hallquist, M., Wenger, J. C., Baltensperger, U., Rudich, Y., Simpson, D., Claeys, M., Dommen, J., Donahue, N. M., George, C., Goldstein, A. H., Hamilton, J. F., Herrmann, H., Hoffmann, T., Iinuma, Y., Jang, M., Jenkin, M. E., Jimenez, J. L., Kiendler-Scharr, A., Maenhaut, W., McFiggans, G., Mentel, Th. F., Monod, A., Prévôt, A. S. H., Seinfeld, J. H., Surratt, J. D., Szmigielski, R., and Wildt, J.: The formation, properties and impact of secondary organic aerosol: current and emerging issues, Atmos. Chem. Phys., 9, 5155–5236, doi:10.5194/acp-9-5155-2009, 2009.

Heald, C. L., Kroll, J. H., Jimenez, J. L., Docherty, K. S., DeCarlo, P. F., Aiken, A. C., Chen, Q., Martin, S. T., Farmer, D. K., and Artaxo, P.: A simplified description of the evolution of organic aerosol composition in the atmosphere, Geophys. Res. Lett., 37, L08803, doi:10.1029/2010GL042737, 2010.

Holzinger, R., Kasper-Giebl, A., Staudinger, M., Schauer, G., and Röckmann, T.: Analysis of the chemical composition of organic aerosol at the Mt. Sonnblick observatory using a novel high mass resolution thermal-desorption proton-transfer-reaction mass-spectrometer (hr-TD-PTR-MS), Atmos. Chem. Phys., 10, 10111–10128, doi:10.5194/acp-10-10111-2010, 2010.

Jokinen, T., Sipilä, M., Junninen, H., Ehn, M., Lönn, G., Hakala, J., Petäjä, T., Mauldin III, R. L., Kulmala, M., and Worsnop, D. R.: Atmospheric sulphuric acid and neutral cluster measurements using CI-APi-TOF, Atmos. Chem. Phys., 12, 4117–4125, doi:10.5194/acp-12-4117-2012, 2012.

Lopez-Hilfiker, F. D., Mohr, C., Ehn, M., Rubach, F., Kleist, E., Wildt, J., Mentel, Th. F., Lutz, A., Hallquist, M., Worsnop, D., and Thornton, J. A.: A novel method for online analysis of gas and particle composition: description and evaluation of a Filter Inlet for Gases and AEROsols (FIGAERO), Atmos. Meas. Tech., 7, 983–1001, doi:10.5194/amt-7-983-2014, 2014.

Matsunaga, A. and Ziemann, P. J.: Gas-Wall Partitioning of Organic Compounds in a Teflon Film Chamber and Potential Effects on Reaction Product and Aerosol Yield Measurements, Aerosol Sci. Tech., 44, 881–892, doi:10.1080/02786826.2010.501044, 2010.

Mentel, Th. F., Wildt, J., Kiendler-Scharr, A., Kleist, E., Tillmann, R., Dal Maso, M., Fisseha, R., Hohaus, Th., Spahn, H., Uerlings, R., Wegener, R., Griffiths, P. T., Dinar, E., Rudich, Y., and Wahner, A.: Photochemical production of aerosols from real plant emissions, Atmos. Chem. Phys., 9, 4387–4406, doi:10.5194/acp-9-4387-2009, 2009.

Mohr, C., Lopez-Hilfiker, F. D., Zotter, P., Prévôt, A. S. H., Xu, L., Ng, N. L., Herndon, S. C., Williams, L. R., Franklin, J. P., Zahniser, M. S., Worsnop, D. R., Knighton, W. B., Aiken, A. C., Gorkowski, K. J., Dubey, M. K., Allan, J. D., and Thornton, J. A.: Contribution of Nitrated Phenols to Wood Burning Brown Carbon Light Absorption in Detling, United Kingdom during Winter Time, Environ. Sci. Technol., 47, 6316–6324, doi:10.1021/es400683v, 2013.

Pankow, J. F.: An absorption model of gas/particle partitioning of organic compounds in the atmosphere, Atmos. Environ., 28, 185–188, doi:10.1016/1352-2310(94)90093-0, 1994.

Renbaum-Wolff, L., Grayson, J. W., Bateman, A. P., Kuwata, M., Sellier, M., Murray, B. J., Shilling, J. E., Martin, S. T., and Bertram, A. K.: Viscosity of α-pinene secondary organic material and implications for particle growth and reactivity, Proceedings of the National Academy of Sciences, 110, 8014–8019, doi:10.1073/pnas.1219548110, 2013.

Riccobono, F., Schobesberger, S., Scott, C. E., Dommen, J., Ortega, I. K., Rondo, L., Almeida, J., Amorim, A., Bianchi, F., Breitenlechner, M., David, A., Downard, A., Dunne, E. M., Duplissy, J., Ehrhart, S., Flagan, R. C., Franchin, A., Hansel, A., Junninen, H., Kajos, M., Keskinen, H., Kupc, A., Kürten, A., Kvashin, A. N., Laaksonen, A., Lehtipalo, K., Makhmutov, V., Mathot, S., Nieminen, T., Onnela, A., Petäjä, T., Praplan, A. P., Santos, F. D., Schallhart, S., Seinfeld, J. H., Sipilä, M., Spracklen, D. V., Stozhkov, Y., Stratmann, F., Tomé, A., Tsagkogeorgas, G., Vaattovaara, P., Viisanen, Y., Vrtala, A., Wagner, P. E., Weingartner, E., Wex, H., Wimmer, D., Carslaw, K. S., Curtius, J., Donahue, N. M., Kirkby, J., Kulmala, M., Worsnop, D. R., and Baltensperger, U.: Oxidation products of biogenic emissions contribute to nucleation of atmospheric particles, Science, 344, 717–721, doi:10.1126/science.1243527, 2014.

Riipinen, I., Yli-Juuti, T., Pierce, J. R., Petäjä, T., Worsnop, D. R., Kulmala, M., and Donahue, N. M.: The contribution of organics to atmospheric nanoparticle growth, Nat. Geosci., 5, 453–458, doi:10.1038/ngeo1499, 2012.

Roldin, P., Eriksson, A. C., Nordin, E. Z., Hermansson, E., Mogensen, D., Rusanen, A., Boy, M., Swietlicki, E., Svenningsson, B., Zelenyuk, A., and Pagels, J.: Modelling non-equilibrium secondary organic aerosol formation and evaporation with the

aerosol dynamics, gas- and particle-phase chemistry kinetic multilayer model ADCHAM, Atmos. Chem. Phys., 14, 7953–7993, doi:10.5194/acp-14-7953-2014, 2014.

Russell, L. M., Bahadur, R., and Ziemann, P. J.: Identifying organic aerosol sources by comparing functional group composition in chamber and atmospheric particles, P. Natl. Acad. Sci., 108, 3516–3521, doi:10.1073/pnas.1006461108, 2011.

Smith, J. N., Barsanti, K. C., Friedli, H. R., Ehn, M., Kulmala, M., Collins, D. R., Scheckman, J. H., Williams, B. J., and McMurry, P. H.: Observations of aminium salts in atmospheric nanoparticles and possible climatic implications, P. Natl. Acad. Sci., 107, 6634–6639, doi:10.1073/pnas.0912127107, 2010.

Veres, P., Roberts, J. M., Warneke, C., Welsh-Bon, D., Zahniser, M., Herndon, S., Fall, R., and de Gouw, J.: Development of negative-ion proton-transfer chemical-ionization mass spectrometry (NI-PT-CIMS) for the measurement of gas-phase organic acids in the atmosphere, Int. J. Mass Spectrom., 274, 48–55, doi:10.1016/j.ijms.2008.04.032, 2008.

Veres, P., Roberts, J. M., Burling, I. R., Warneke, C., de Gouw, J., and Yokelson, R. J.: Measurements of gas-phase inorganic and organic acids from biomass fires by negative-ion proton-transfer chemical-ionization mass spectrometry, J. Geophys. Res., 115, D23302, doi:10.1029/2010JD014033, 2010.

Volkamer, R., Jimenez, J. L., San Martini, F., Dzepina, K., Zhang, Q., Salcedo, D., Molina, L. T., Worsnop, D. R., and Molina, M. J.: Secondary organic aerosol formation from anthropogenic air pollution: Rapid and higher than expected, Geophys. Res. Lett., 33, L17811, doi:10.1029/2006GL026899, 2006.

Williams, B. J., Goldstein, A. H., Kreisberg, N. M., and Hering, S. V.: An In-Situ Instrument for Speciated Organic Composition of Atmospheric Aerosols: Thermal Desorption Aerosol GC/MS-FID (TAG), Aerosol Sci. Tech., 40, 627–638, doi:10.1080/02786820600754631, 2006.

Yasmeen, F., Vermeylen, R., Szmigielski, R., Iinuma, Y., Böge, O., Herrmann, H., Maenhaut, W., and Claeys, M.: Terpenylic acid and related compounds: precursors for dimers in secondary organic aerosol from the ozonolysis of α- and β-pinene, Atmos. Chem. Phys., 10, 9383–9392, doi:10.5194/acp-10-9383-2010, 2010.

Yatavelli, R. L. N., Lopez-Hilfiker, F., Wargo, J. D., Kimmel, J. R., Cubison, M. J., Bertram, T. H., Jimenez, J. L., Gonin, M., Worsnop, D. R., and Thornton, J. A.: A Chemical Ionization High-Resolution Time-of-Flight Mass Spectrometer Coupled to a Micro Orifice Volatilization Impactor (MOVI-HRToF-CIMS) for Analysis of Gas and Particle-Phase Organic Species, Aerosol Sci. Tech., 46, 1313–1327, doi:10.1080/02786826.2012.712236, 2012.

Yatavelli, R. L. N., Stark, H., Thompson, S. L., Kimmel, J. R., Cubison, M. J., Day, D. A., Campuzano-Jost, P., Palm, B. B., Hodzic, A., Thornton, J. A., Jayne, J. T., Worsnop, D. R., and Jimenez, J. L.: Semicontinuous measurements of gas–particle partitioning of organic acids in a ponderosa pine forest using a MOVI-HRToF-CIMS, Atmos. Chem. Phys., 14, 1527–1546, doi:10.5194/acp-14-1527-2014, 2014.

Zhao, Y., Kreisberg, N. M., Worton, D. R., Isaacman, G., Weber, R. J., Liu, S., Day, D. A., Russell, L. M., Markovic, M. Z., Van den Boer, T. C., Murphy, J. G., Hering, S. V., and Goldstein, A. H.: Insights into Secondary Organic Aerosol Formation Mechanisms from Measured Gas/Particle Partitioning of Specific Organic Tracer Compounds, Environ. Sci. Technol., 47, 3781–3787, doi:10.1021/es304587x, 2013.

Ziemann, P. J.: Evidence for Low-Volatility Diacyl Peroxides as a Nucleating Agent and Major Component of Aerosol Formed from Reactions of O_3 with Cyclohexene and Homologous Compounds, J. Phys. Chem. A, 106, 4390–4402, doi:10.1021/jp012925m, 2002.

Ziemann, P. J. and Atkinson, R.: Kinetics, products, and mechanisms of secondary organic aerosol formation, Chem. Soc. Rev., 41, 6582, doi:10.1039/c2cs35122f, 2012.